Title
DISSOCIATION OF HYDROGEN ON TAMPALUM USING MODULATED MOLECULAR BEAM TECHNIQUE

Author
Krakowski, Robert A.

Publication Date
1967-03-01

UCRL-17336 (Rev.)

eg. 2

University of California

Ernest O. Lawrence Radiation Laboratory

DISSOCIATION OF HYDROGEN ON TANTALUM
USING A MODULATED MOLECULAR BEAM TECHNIQUE

R. A. Krakowski and D. R. Olander

June 1967

Berkeley, California

DISCLAIMER

Submitted to J. Chem. Phys.

UCRL-17336 Rev.
Preprint

UNIVERSITY OF CALIFORNIA

Lawrence Radiation Laboratory
Berkeley, California

AEC Contract No. W-7405-eng-48

DISSOCIATION OF HYDROGEN ON TANTALUM USING A MODULATED MOLECULAR BEAM TECHNIQUE

R. A. Krakowski and D. R. Olander

June 1967

UCRL-17336 Rev.

DISSOCIATION OF HYDROGEN ON TANTALUM USING A MODULATED MOLECULAR BEAM TECHNIQUE

R. A. Krakowski and D. R. Olander

Inorganic Materials Research Division, Lawrence Radiation Laboratory, and the Department of Nuclear Engineering, College of Engineering, University of California, Berkeley, California

ABSTRACT

A molecular beam-mass spectrometric apparatus has been developed to study the kinetics of gas-solid reactions at low pressures. The system has been used in an investigation of the dissociation of hydrogen on tantalum. A modulated beam of molecular hydrogen, formed by effusion from a high pressure source, impinged upon the tantalum target. The reflected H_2 and H atoms emitted after surface dissociation were monitored by a mass spectrometer in the vacuum system. The beams were modulated and the products measured by a phase-sensitive detector to improve the signal-to-noise characteristics of the detection system. The degree of dissociation was studied as a function of the surface temperature, beam temperature, and beam intensity. Experimental results have been analyzed in terms of phenomenological first and second order kinetic models. Within the pressure (3×10^{-8} - 3×10^{-7} torr) and temperature (1000 to 2500°K) ranges studied, the data agreed best with the first order mechanism, and yielded 65 kcal/mole for the hydrogen-metal bond energy. At a given temperature, dissociation increased with the beam temperature with an apparent activation energy of 1.4 kcal/mole, which was independent of

---

* Present address: Chemistry Department, EURATOM, Ispra, Italy.

the surface temperature. The rate of dissociation varied linearly with the beam intensity. Mixed hydrogen-deuterium beams were employed to investigate the isotope exchange reaction, and, within the sensitivity of the detection system, exchange did not take place. A simple kinetic model, which proposes a high adatom recombination probability before significant surface diffusion occurs, was proposed to explain the observed first order kinetics. Hydrogen solubility in the metal bulk has been considered as a possible source for the observed non-equilibrium behavior.

INTRODUCTION

Detailed information on the interactions of gases with solid surfaces is important to the elucidation of the mechanisms of processes such as energy exchange, chemical catalysis, corrosion, ablation and adsorption. The interaction of diatomic gases with chemically inert surfaces is one of the simplest systems for experimental studies of this nature. Over the last half century hydrogen-metal systems have received considerable attention. Dissociative adsorption of hydrogen on metals is the first step in bulk diffusion and hydriding phenomena, which are of practical importance in the problem of hydrogen embrittlement of reaction fuel element cladding.

The experimental history of the hydrogen-metal interaction reveals continual improvement in the definition and measurement of the system variables. Langmuir,[1,2,3] in his classical work on the interaction of hydrogen with hot tungsten filaments by the flash filament technique, relied solely on the decrease of the total pressure due to the highly efficient pumping of atomic hydrogen by the cooled walls of the reaction vessel.

This work gave a value for the hydrogen dissociation energy which agreed well with the spectroscopic values of Giaugue[4] and led to the now famous theory of monolayer adsorption, but many side-effects remained unresolved. Although recent advances in vacuum technology and electronics have permitted great refinements in flash filament techniques,[5,6] two major uncertainties remain: 1) the nature of the reaction products emitted from the surface is unknown, since total pressure changes are used to measure the degree of dissociation; 2) because the background gas in the

vacuum chamber is the source of impinging molecules, little control over the temperature and degree of dissociation of the incident molecules is possible.

The advent of accurate mass spectrometric techniques has provided the means of eliminating the first of these limitations. Bergsnov-Hansen and Pasternak[7] employed a mass spectrometer in conjunction with a hot molybdenum filament to investigate the hydrogen-deuterium isotope exchange reaction. Direct measurement of emitted reaction products was made by Moore and Unterwald[8,9] who used a mass spectrometer to investigate the hydrogen dissociation reaction at various refractory metal surfaces. While uncertainties associated with the identity of the reaction products were eliminated, the source of impinging molecules was still obtained from the background gas in the vacuum system.

The use of molecular beams in conjunction with mass spectrometric detection affords strict control of the composition and temperature of incident reactant molecules. The hydrogen-tungsten system was investigated in this manner by Smith and Fite[10,11] who used a modulated beam technique in order to achieve improved signal-to-noise ratios. The primary advantages of the modulated molecular beam experiment have been discussed by Holister, Brackmann and Fite.[12] Other systems have been studied by similar techniques.[13,14,15,16] Although considerable work has been done on the interaction of hydrogen with other refractory metals (tungsten and molybdenum), rhenium, platinum and carbon, the hydrogen-tantalum system has not been investigated. Unique features of this system are the large solubility of hydrogen in the metal and the stability of the hydride, which could alter the dissociation mechanism established for metals such as tungsten.

EXPERIMENTAL

A molecular beam of known intensity and temperature is generated by gas flow through an array of long narrow channels, modulated by a mechanical chopper, and directed at a solid target. A small portion of the products of the gas-solid interaction which leave the target pass through the ionizer of a mass spectrometer without collisions with solid surfaces or molecules in the gas phase. The output of the mass spectrometer is amplified by a phase sensitive detector. A detailed description of the experimental method is given in Ref. 17, and only a summary is presented here.

Figure (1) shows a schematic drawing of the two chamber, differentially pumped vacuum system used in the experiment. The source chamber houses a multi-channel source of the "krinkly foil" type[18] capable of heating to 1800°K by electron bombardment. By means of a specially designed bellows mounting device, the Knudsen cell source can be externally aligned with respect to the collimation apertures. Viewing ports provide an optical line-of-sight along the entire beam path and permit alignment of the system by a small gas laser. Temperature measurement of the inner face of the multi-channel source was made by optical pyrometry. Gas is supplied to the Knudsen cell through palladium leak or by precision mechanical leak for mixed beams. The mercury diffusion pump on the source chamber has an effective speed estimated at 100 ℓ/sec, which maintained a pressure of $\sim 10^{-4}$ torr in the source chamber when the strongest beams were used. The base pressure in the source chamber is 2×10^{-7} torr.

Effusing molecules from the multi-channel source are collimated by a small aperture separating the source chamber from the experimental

chamber which is provided with 1200 liters/second of ion pumping. The pressure in the experimental chamber increases from a no-load value of 5×10^{-9} torr to 3×10^{-7} torr when the beam of maximum intensity is generated (source pressure = 3 torr). The experimental chamber contains the beam chopper, second collimation aperture, the beam monitor, tantalum target, and the quadrupole mass spectrometer. Figure (2) gives the details of the beam geometry and illustrates the collimation, modulation, interaction, and detection processes, as well as all pertinent dimensions.

The 0.001-inch target foil is resistively heated with dc current and is mechanically positioned with a linear feed through. A uniform temperature area 1 cm × 2 cm is exposed to the beam. The target temperature is measured optically through the viewing port on the right of Fig. (1). The target was outgassed at 1800°C before each measurement. The beam is mechanically interrupted by a two blade chopper motor prior to final collimation. The chopper is driven at a modulation frequency of 50 cps by a hysteresis synchronous motor located in the experimental chamber. The modulated beam traverses the second collimator and passes through a small ionizer of the Pierce gun variety. The output from this "beam monitor ionizer" is amplified and displayed on an oscilloscope to give a relative measure of beam intensity. The chopping frequency is obtained from a light-photodiode arrangement.

After the beam interacts with the target, reflected species are detected with a small quadrupole mass spectrometer, which is located at an angle of 45° with respect to the target normal. The output from a 16 stage Cu(Be) electron multiplier of the mass spectrometer is fed to the high impedence input (10^7 ohms) of a phase-sensitive, lock-in detector

which is referenced in time to the signal from the photodiode at the chopper motor. The filtered output from the lock-in amplifier is monitored with a variable speed strip-chart recorder. No phase shifts were measurable. At a chopping frequency of 50 cps, a minimum time lag of ~ 170 μsec is detectable. Molecular transit times in the apparatus were 20-50 μsec and thus not resolvable.

In most experiments, the pressure in the Knudsen cell was 3 torr. The beam generated by this source pressure at 300°K is referred to as the "standard beam", and corresponds to an intensity at the target of approximately 4×10^{14} molecules/cm^2-sec.[17] The equivalent pressure of the standard beam (in terms of rate of impingement on a surface) is 3×10^{-7} torr. The pressure in the experimental chamber under these beam conditions was also 3×10^{-7} torr, and consisted of over 90% H_2. It will be convenient to refer to a beam-to-background impingement rate ratio defined by

$$\rho = \frac{I_T^0}{I^{bkg}} \qquad (1)$$

where I_T^0 is the amplitude of the modulated beam intensity at the location of the target and I^{bkg} is the impingement rate of background gas per square cm of target. For the standard beam, ρ was (fortuitously) unity.

The beam intensity (as measured by the beam monitor ionizer) was found to vary with the square root of the leak rate (measured by the source pressure) as predicted by theory.[19,20] The background pressure (or I^{bkg}) was directly proportional to the leak rate, since the primary gas load on the experimental chamber was due to effusion of the non-directed molecules from the source chamber through the small collimating orifice between the

two chambers. For beams weaker than the standard beam, the signal-to-background ratio was larger than unity and expressible by

$$\rho = \frac{\left(I_T^0\right)_{std}}{I_T^0} \qquad (2)$$

This ratio was directly measurable by the beam monitor ionizer.

Reflection of the standard beam from the target produced a beam of $\sim 3\times10^{12}$ molecules/cm^2-sec intensity in the ionizer of the mass spectrometer[17]; this intensity is equivalent to a pressure of $\sim 5\times10^{-10}$ torr in terms of number density. The signal-to-background figure at this location was at most 10^{-3}, which clearly indicates the necessity of phase-sensitive detection.

Treatment of Signals

The species i, reflected (or emitted) from the target, ionized, and mass analyzed, produces a modulated (ac) signal, $S_i(t)$, which is related to the surface emission $R_i^E(t)$ (molecules/cm^2-sec) by:

$$S_i(t) = \alpha_i R_i^E(t)/\sqrt{T_i} \qquad (3)$$

where T_i is the temperature at which the ith species leaves the surface. The term $\sqrt{T_i}$ reflects the influence of the mean velocity of the neutral particle on the efficiency of ionization in the mass spectrometer. α_i denotes a system-dependent constant which contains geometric factors, ionization cross-sections, and detection efficiencies.

The rate at which a particular species is emitted from the surface depends upon the rate of impingement of reactant gas on the target via some kinetic mechanism. The total impingement rate contains an ac

contribution from the modulated primary beam and a dc component from the background gas, which consists predominantly of the same species as in the primary beam. Even though the background component is unmodulated, it influences the rate of product emission by contributing to the supply of adsorbed atoms in the surface. Only in the case of a first order surface mechanism does the phase sensitive detector completely remove the undesirable dc component.

In order to reveal the effect of the background gas on the output signal, the total rate of impingement on the target is written as

$$I_T = I_T^O\left[f(t) + 1/\rho\right] \qquad (4)$$

The periodic function f(t) represents the modulation of the primary beam, and varies from zero to unity. In these experiments, f(t) was observed to be nearly a square wave.

The lock-in detector produces a dc output which is proportional to the amplitude of the ac input. The operation of the lock-in detector can be represented as a process whereby cosine averaging an ac input signal yields a dc output. For the case of zero phase-lag between the reference signal and the input signal dc output is:

$$\bar{S}_i = \frac{1}{\tau}\int_0^{\tau} S_i(t) \cos 2\pi f_0 t \, dt \qquad (5)$$

where τ is the filtering time constant of the lock-in detector and f_0 is the modulation frequency ($1/\tau \ll f_0$). Since the ac component of $S_i(t)$ is adequately represented by a square wave, and $S_i(t)$ is proportional to $R_i^E(t)$

according to Eq. (3), the cosine average $\tilde{S}_i$ is proportional to the difference between the maximum and minimum of $R_i^E(t)$. Any term in $S_i(t)$ which can be considered an additive constant will be null-averaged by Eq. (5). For a square wave, the cosine average is performed only on the first harmonic, and the resulting constant depression factor of $2/\pi$ can be absorbed into α_i. Inserting Eq. (3) into Eq. (5) yields

$$\tilde{S}_i = \frac{\alpha_i}{\sqrt{T_i}} \left\{ R^E_{i(max)} - R^E_{i(min)} \right\} . \qquad (6)$$

It is readily seen that if R_i^E is first order with respect to the impingement rate, I_T, the $1/\rho$ term in Eq. (4) cancels in Eq. (6). The output $\tilde{S}_i$ is independent of the background contribution. For the case of nonlinear dependence of the rate on the beam intensity, the final output signal will not be independent of ρ; an analytical surface model must be used to obtain the dependence of R_i^E on I_T and the resulting expression then substituted into Eq. (6), which will exhibit an explicit ρ dependence.

First and Second Order Kinetics

A minimum of three surface steps is required to describe the dissociation process: dissociative adsorption of a fraction of the molecules impinging on the surface; atom evaporation from the surface; and molecular reconstitution and evaporation.

At low surface coverage, the rate of H_2 adsorption can be described by

$$R_2^A = \eta_2 I_T \qquad (7)$$

where η_2 is the temperature-independent sticking coefficient.[5,6,8,9]

The rate of atom emission from the surface is

$$R_1^E = k_1^E n \tag{8}$$

The rate constant for atom evaporation is denoted by k_1^E, and n refers to the surface concentration of adsorbed atoms.

Molecular hydrogen is evaporated from the surface according to

$$R_2^E = k_2^E n^m \tag{9}$$

The exponent m in Eq. (9) is two for second order (equilibrium) molecular desorption. If molecular evaporation is first order in surface concentration, m is unity. The rate constant for this step is denoted by k_2^E.

The three rates are subject to the surface material balance

$$R_2^A = R_2^E + \tfrac{1}{2}R_1^E \tag{10}$$

Combining Eqs. (7-10) and solving for R_1^E yields

$$R_1^E = \frac{\left(k_1^E/k_2^E\right)\eta_2 I_T}{\frac{1}{2}\left(k_1^E/k_2^E\right) + 1}, \quad \text{for} \quad m = 1 \tag{11}$$

$$R_1^E = \tfrac{1}{4}\frac{\left(k_1^E\right)^2}{k_2^E}\left[\sqrt{1 + \frac{16\eta_2 I_T}{\left(k_1^E\right)^2/k_2^E}} - 1\right], \text{ for } m = 2 \tag{12}$$

Both atomic hydrogen emitted from the surface and molecular hydrogen which has been reconstituted and evaporated from the surface are assumed to have

attained the temperature of the solid substrate. Using Eq. (4), substitution of Eqs. (11) and (12) into Eq. (6) yields

$$\sqrt{T_T}\,\tilde{S}_1 = \alpha_1 \frac{\left(k_1^E/k_2^E\right)\eta_2 I_T^0}{\frac{1}{2}\left(k_1^E/k_2^E\right) + 1}, \quad \text{for } m = 1 \tag{13}$$

$$\sqrt{T_T}\,\tilde{S}_1 = \frac{4\alpha_1\eta_2 I_T^0}{b}\left[\sqrt{1 + b\left(1 + \frac{1}{\rho}\right)} - \sqrt{1 + \frac{b}{\rho}}\right], \quad \text{for } m = 2 \tag{14}$$

where

$$b = \frac{16\eta_2 I_T^0}{\left(k_1^E\right)^2/k_2^E} \tag{15}$$

If in addition to the requirement of second order the ratio of the H and H_2 emission rates is assumed to be that of a surface in equilibrium with a suitable gas phase, the ratio $\left(k_1^E\right)^2/k_2^E$ can be expressed in terms of the gas phase equilibrium constant by means of the principle of detailed balance.[21] For equilibrium second order emission, the parameter b becomes

$$b = \frac{8\eta_2\eta_2^{eq}}{\left(\eta_1^{eq}\right)^2} \frac{\left(2\pi m_2 k T_T\right)^{1/2} I_T^0}{K_p\left(T_T\right)} \tag{16}$$

where $K_p\left(T_T\right)$ is the thermodynamic equilibrium constant for the reaction $H_2(g) = 2H(g)$ at the temperature of the target, T_T. η_1^{eq} and η_2^{eq} are sticking coefficients for H and H_2 respectively under equilibrium conditions (i.e., gas and surface at T_T).

Eq. (14) for the second-order model contains the beam-to-background ratio, ρ, but in the first-order model this effect is absent.

Similar expressions can be obtained for the rate of emission of molecular hydrogen. However, the temperature of the portion of the incident H_2 which is reflected without adsorption depends upon the extent of thermal accommodation with the surface.

RESULTS AND DISCUSSION

Typical traces of the output of the phase-sensitive detector as the target temperature was varied are shown on Fig. (3). Both the mass one and mass two signals dropped to the noise level when either the target was removed from the path of the beam, or the beam was shut off. The noise level was approximately 1% of the maximum signal. The mass one background observed with a cold target was due to the cracking of the reflected H_2 in the ionizer of the mass spectrometer.

In order to assess the validity of the models discussed previously, four parameters were varied: 1) the target temperature T_T; 2) the beam temperature T_B; 3) the beam intensity I_T^0; and 4) the composition of the beam. The results of these experiments were interpreted in terms of Eqs. (13) and (14) (or the equivalent equations for H_2). The instrumental constant in these relations is difficult to calculate and was subject to variation from one experiment to another (due to electron multiplier gain drift, background pressure fluctuations, and variations in electronic settings). Consequently, all signals were normalized by reference to the signal obtained in the same experiment when the parameter under investigation took on its highest or lowest value.

Effect of Target Temperature

The standard beam (3 torr source pressure, 300°K source temperature) was employed in all experiments involving variation of target temperature.

Beyond 2300°K, both the mass one and mass two signals were independent of temperature. The atomic hydrogen signal has been normalized with respect to the high temperature limit and expressed as

$$S_1 = \frac{\sqrt{T_T}\,\bar{S}_1}{\left[\sqrt{T_T}\,\bar{S}_1\right]_{T_T \to \text{large}}} \qquad (17)$$

Figure 4 shows the results of seven experiments with the standard beam. Atomic hydrogen was first observed at 1400°K; below this temperature, all hydrogen chemisorbed from the beam evaporated as H_2. Above 2300°K, evaporation of atomic hydrogen was the sole mode of desorption. Between these limits, molecular and atomic hydrogen evaporation are of comparable magnitudes. Experiments 2, 3d, 5a, and 5b utilized a new tantalum target. The remaining three experiments were performed with the same foil after a period of several months during which the target had been subjected to long periods at elevated temperatures and to exposure to CO purposely introduced into the beam. Microscopic and chemical examination of this "old" target showed considerable grain growth and a substantial increase in carbon content. Yet, as seen from Fig. 4, the hydrogen emission characteristics of the target was the same in the old and new conditions. In one experiment (No. 16g), a beam containing 5% CO was employed. This is equivalent to a CO partial pressure of ~ 10^{-8} torr, which is approximately an order of magnitude greater than the CO in the experimental chamber gas as estimated from the background mass spectrum. The emission of atomic hydrogen was unaffected by the addition of 5% CO to the primary beam.

The H_2 signal has been normalized by dividing $\bar{S}_2$ by its value for a room temperature target

$$S_2 = \frac{\bar{S}_2}{\left[\bar{S}_2\right]_{T_T = 300°K}} \qquad (18)$$

The variation of s_2 with T_T measured in seven experiments (different from those in which atomic hydrogen was monitored) is shown in Fig. (5). Contrary to the emission of atomic hydrogen, the evaporation and/or reflection of molecular hydrogen was distinctly different for the "old" and "new" targets.

At the temperature at which the plateau occurred (~ 2300°K), the H_2 emanating from the target is due only to the fraction $1-\eta_2$ which is reflected without adsorption. The decrease in the mass two signal at high temperatures is a result of three effects: 1) the removal from the beam of the fraction η_2 which has been chemisorbed on the target and re-evaporated as atoms; 2) partial thermal accommodation of the reflected portion of the beam, which increases the temperature of the reflected H_2 above 300°K and decreases the efficiency of detection according to Eq. (6); and 3) the change of the angular distribution of the reflected H_2 from diffuse at low temperatures to specular at high temperatures.[11,13] Since the process of reflection of H_2 from the target is first order in the impingement rate, the bracketed term in Eq. (6) represents the fraction of the primary modulated H_2 beam reflected from the target. The normalized H_2 signal at the high temperature plateau can be expressed by

$$\left[s_2\right]_{T_T \to \text{large}} = \left(1 - \eta_2\right)\sqrt{\frac{300}{T_2}}\left(\frac{\alpha_2^{spec}}{\alpha_2^{diff}}\right) \qquad (19)$$

where T_2 is the temperature of the reflected H_2 and α_2^{spec} and α_2^{diff} are the coefficients in Eq. (6) for specular and diffuse reflection.

The specular reflection patterns observed by Datz et al.[13] and Smith and Fite[11] can be represented by ellipses. For normal incidence, the

ratio $\alpha_2^{spec}/\alpha_2^{diff}$ depends upon the eccentricity of the ellipse and the angle of observation with respect to the target normal according to[17]

$$\frac{\alpha_2^{spec}}{\alpha_2^{diff}} = \frac{1 - \epsilon^2 \cos^2 \theta}{\left(1 - \epsilon^2\right)^{3/4}} \qquad (20)$$

where ϵ is the eccentricity of the elliptical reflection pattern and θ is the angle with respect to the target normal, which is the same as the direction of incidence. Equation (20) represents the ratio of the reflected intensity from an elliptical pattern to that from a cosine distribution at an angle θ and for the same total emission rate.

The plateaus on Fig. 5 correspond to sticking probabilities of 0.49 and 0.70 for the new and old targets respectively if the effects of thermal accommodation and specular reflection are ignored. An indication of the magnitude of these effects can be seen from the results of Smith and Fite for H_2 scattering from tungsten. They found a thermal accommodation coefficient of 0.07 and a specular reflection pattern at $T_T = 2500°K$ which can be characterized by an ellipse of eccentricity ~ 0.6. Assuming these figures to apply to a 2300°K tantalum target, the calculated temperature of the reflected beam is ~ 440°K, which results in a 21% reduction in the signal due to thermal accommodation. The alpha ratio for a specular pattern characterized by $\epsilon = 0.6$ and an observation angle of 45° provides an additional 11% reduction in the H_2 signal. Applying these corrections to Eq. (19), the sticking probability for the new target is reduced from 0.49 to 0.30. The depression of the curve on Fig. 5 for the old target may be the result either of improved thermal accommodation of the reflected beam due to the carbon impurities on the surface or of increased specular reflection caused

by the growth of large grains. The difference in the curves of Fig. 5 may not represent a real alteration in the sticking probability between the target in the two conditions.

Although the sticking probabilities implied by the plateaus of Fig. 5 (uncorrected) are higher than those reported for similar materials, the values measured for other refractor metals show large variations. Smith and Fite[11] obtained 0.30 for tungsten, while Hickmott's measured value was 0.05.[22] Moore and Unterwald,[9] working with molybdenum, corroborated Langmuir's earlier value of 0.49, obtained with tungsten. Bergsnov-Hansen and Pasternak[7] observed 0.4 at 720°K and 0.15 at 300°K with molybdenum. We do not know the extent to which our observed values of 0.49 and 0.70 are too high because of thermal accommodation and specular reflection of the non-chemisorbed H_2, but in any case these figures constitute an upper limit on the sticking probability of H_2 on tantalum.

The interpretation of the atom emission data is not beset by the same uncertainties, since the temperature of the evaporated atoms is equal to the target temperature and the angular distribution is diffuse.[11]

In terms of the model discussed earlier, the dominance of atom emission over molecular evaporation at high temperatures implies that $k_1^E \gg k_2^E$. Both Eqs. (13) and (14) reduce to $2\alpha_1\eta_2 I_T^0$. Dividing this expression into Eq. (14) gives the theoretical prediction of the normalized H signal according to the second order model

$$s_1 = \frac{2}{b_{std}}\left[\sqrt{1 + b_{std}\left(1 + \frac{1}{\rho}\right)} - \sqrt{1 + \frac{b_{std}}{\rho}}\right] \qquad (21)$$

where b_{std} is given by Eq. (15) with I_T^0 replaced by the intensity of the

standard beam used in the experiments, $\left(I_T^0\right)_{std}$. For equilibrium second order dissociation, b_{std} is given by Eq. (16).

Assuming $\rho = 1$, the s_1 values from the smooth curve of Fig. 4 can be converted to an experimental value of b_{std} by Eq. (21). The equilibrium second order value of b_{std} is obtained from Eq. (16) with a beam intensity of 4×10^{14} molecules/cm^2-sec, $\eta_2 = \eta_2^{eq} = 0.49$ (the uncorrected value for the new target), $\eta_1^{eq} = 1.0$, and $K_p(T_T)$ from the literature compilation.[23] Comparison of the experimental and calculated equilibrium values of b_{std} are shown in Fig. 6. The calculated values are approximately three orders of magnitude below those obtained from the data. For molybdenum, however, Moore and Unterwald[9] found good agreement with a calculation equivalent to Eq. (21), although comparable agreement with theory for a tungsten surface was not obtained. Hickmott,[22] using his measured sticking probability of 0.05, was able to obtain reasonable agreement with the equilibrium second order model if the sticking probability for atomic hydrogen was taken as ~ 0.16. In our case, accord between theory and experiment would require $\eta_1^{eq} \approx 0.03$. While recent evidence suggests that the sticking coefficient of H may be smaller than that for H_2,[24] a value as low as 0.03 seems unreasonable. Although the experimental values of ρ, η_2 and $\left(I_T^0\right)_{std}$ are not known with great accuracy, they are not low by three orders of magnitude.

Equation (13) for first order H_2 surface reconstitution can be written as

$$s_1 = \frac{\frac{1}{2}\left(k_1^E/k_2^E\right)}{\frac{1}{2}\left(k_1^E/k_2^E\right) + 1} \qquad (22)$$

The data for the seven experiments in which H was monitored are plotted as the rate constant ratio vs $1/T_T$ in Fig. 7; Eq. (22) has been used to convert s_1 to k_1^E/k_2^E. There is a break in the curve at a target temperature of 1800°K. Above this temperature, the activation energy of the rate constant ratio is 42 kcal/mole.

The first order model can also be used to obtain a relation between k_1^E/k_2^E and s_2. Neglecting thermal accommodation and specular reflection effects for the non-adsorbed H_2, there results

$$R_2 = \left(1 - \eta_2\right) + \eta_2 \left[\frac{1}{\frac{1}{2}\left(k_1^E/k_2^E\right) + 1}\right] \quad . \tag{23}$$

The normalized data for the seven experiments in which H_2 was measured have been converted to the rate constant ratio by use of Eq. (23). In so doing, the uncorrected η_2 appropriate to the condition of the target in each run was used (i.e., the target was either new or old, and the sticking probability was taken as either 0.49 or 0.70). The results are shown on Fig. 8. Despite the scatter of the data, both the slope and magnitude of the line agree well with the line on Fig. 7 for $T_T > 1800$°K. The two plots utilize independent data which were obtained in different experiments. Notwithstanding the insecurity of the H_2 data due to neglect of thermal accommodation and specular reflection, the agreement between Figs. 7 and 8 indicates that the two sets of measurements are consistent with a first order surface model.

The rate constants can be written as[21]

$$k_1^E = \nu_1 e^{-\chi/kT_T} \tag{24}$$

and

$$k_2^E = \nu_2 e^{-V/kT_T} \tag{25}$$

where X is the energy difference between an adsorbed atom and a free gas atom and V is the energy difference between two adsorbed atoms and a molecule of gaseous H_2. These energies are related to the dissociation energy of the gaseous molecule by

$$2\chi - V = D \tag{26}$$

The 42 kcal/mole activation energy characteristic of the line of Fig. 8 and the high temperature portion of the line of Fig. 7 represent X - V. Using D = 103 kcal/mole, we obtain X = 65 kcal/mole. Ehrlich[21] gives a value of 74 kcal/mole for this parameter while Hickmott[22] has measured X = 67 kcal/mole for tungsten.

Effect of Beam Temperature

The variation in the mass one signal as the temperature of the primary beam was increased from 1150°K to 1800°K for various target temperatures was measured and compared to the results for a room temperature beam. The strength of the beam was equal to that of the standard beam. The results are shown in Fig. 9.

For a fixed value of T_T, the mass one signal at an elevated beam temperature has been normalized by division by the corresponding value at the same target temperature with a 300°K beam

$$\zeta_1 = \frac{\bar{S}_1(T_B, T_T)}{\bar{S}_1(300, T_T)} \tag{27}$$

The increase of ζ_1 with T_B is attributed to the ability of the more energetic, hotter molecules to overcome a small activation energy barrier separating the gaseous and adsorbed states. In accord with most other investigations, the sticking probability is assumed independent of target temperature. The variation with beam temperature is taken to be of the form

$$\eta_2(T_B) = c\, e^{-E_a/kT_B} \tag{28}$$

where E_a is the activation energy for dissociative adsorption and C is a temperature-independent constant.

In applying the second order model represented by Eqs. (14) and (15) to these data, the sticking probability appears only in the bracketed term of Eq. (14) via the parameter b. For beam temperatures other than 300°K, b can be written as $b_{std}\eta_2(T_B)/\eta_2(300)$, since the beam strength in this experiment was that of the standard beam. Using Eq. (14) with $\rho = 1$, the normalized mass one signal is

$$\zeta_1 = \frac{\sqrt{1 + 2b_{std}\dfrac{\eta_2(T_B)}{\eta_2(300)}} - \sqrt{1 + b_{std}\dfrac{\eta_2(T_B)}{\eta_2(300)}}}{\sqrt{1 + 2b_{std}} - \sqrt{1 + b_{std}}} \tag{29}$$

at high target temperatures ($b_{std} \to 0$), Eq. (29) reduces to

$$\left[\zeta_1\right]_{T_T \to \text{large}} = \frac{\eta_2(T_B)}{\eta_2(300)} = \left[\frac{c}{\eta_2(300)}\right] e^{-E_a/kT_B} \tag{30}$$

At low target temperatures ($b_{std} \to \infty$), the limit is

$$\left[\zeta_1\right]_{T_T \to 0} = \sqrt{\frac{\eta_2(T_B)}{\eta_2(300)}} = \left[\frac{c}{\eta_2(300)}\right]^{1/2} e^{-\frac{1}{2}E_a/kT_B} \quad (31)$$

According the Eqs. (30) and (31), Arrhenius plots of the ζ_1-T_B data should show a maximum activation energy at high target temperatures. As the target temperature is reduced, the activation energy should decrease, approaching one-half of the maximum value at very low target temperatures. Equation (29) can be used as an interpolation formula for intermediate T_T. Figure 10 compares the data and the predicted variation of ζ_1 with T_T according to the second order model. The constants $c/\eta_2(300)$ and E_a have been computed from the high target temperature data on Fig. (9) in conjunction with Eq. (30). The intermediate lines have been computed from Eq. (29) and the experimental values of b_{std} from Fig. 6. The $T_T = 0°K$ line represents Eq. (31).

There is no suggestion that the activation energy of ζ_1 decreases with decreasing target temperature, as required by the second order model. On the contrary, the points for all target temperatures are best represented by a single line with an activation energy of 1.4 kcal/mole. This behavior is consistent with the first order model (Eq. (10), which for all target temperatures yields

$$\zeta_1 = \left[\frac{c}{\eta_2(300)}\right] e^{-E_a/kT_B} \quad (32)$$

The activation energy of 1.4 kcal/mole is valid only for $1150 < T_B < 1800°K$, since the upper line of Fig. 10 does not pass through $\zeta_1 = 1$ at $T_B = 300°K$.

Effect of Beam Intensity

The variation of beam intensity is equivalent to variation of the reactant gas pressure in experiments utilizing the randomly directed gas in a reaction chamber. It is perhaps the most direct method of ascertaining the order of the reaction.

In this series of experiments, the beam temperature was always 300°K. In one experiment, the beam intensity was varied from 10% of the intensity of the standard beam to the full strength of the standard beam. The target was maintained at 1980°K. At this temperature, Fig. 4 indicates that the H signal was about one-half of the plateau value. This is well within the region where second order effects, if present, would be observed. The results of this experiment are shown in Fig. 11. The abscissa represents the output signal of the beam monitor ionizer, which is proportional to the beam strength. Except for the highest beam intensities, the variation of $\bar{S}_1$ with V_B is linear. In another experiment, the variation of the H signal with target temperature was measured for four beam intensities. These results are shown on Fig. 12. For comparison with the first and second order models, the H signal has been normalized to the value for the standard beam

$$\theta_1 = \frac{\bar{S}_1\left(I_T^0\right)}{\bar{S}_1\left[\left(I_T^0\right)_{std}\right]} \tag{33}$$

The ratio $I_T^0/\left(I_T^0\right)_{std}$ is a convenient measure of the beam strength. The inverse of this ratio is, according to Eq. (2), the signal-to-background ratio, ρ. The parameter $1/\rho$ provides a single variable for denoting both the relative beam strength and the signal-to-background ratio. In the latter role, ρ appears explicitly in the formula for the second

order model, Eq. (14). As a measure of beam intensity, it appears in the parameter b of Eq. (15), which can be written in terms of b_{std} by

$$b = b_{std} \frac{I_T^0}{\left(I_T^0\right)_{std}} = \frac{b_{std}}{\rho} \tag{34}$$

Inserting Eq. (34) into Eq. (14) and dividing the resulting equation by its value for $\rho = 1$ gives

$$\theta_1 = \frac{\sqrt{1 + b_{std} \frac{1}{\rho}\left(1 + \frac{1}{\rho}\right)} - \sqrt{1 + b_{std} \frac{1}{\rho^2}}}{\sqrt{1 + 2b_{std}} - \sqrt{1 + b_{std}}} \tag{35}$$

Equation (35) is the predicted variation of θ_1 with $1/\rho$ according to the second order model. In the limit of high target temperature ($b_{std} \to 0$), it reduces to a pseudo-first order form

$$\left[\theta_1\right]_{T_T \to \text{large}} = 1/\rho \tag{36}$$

at low temperatures ($b_{std} \to \infty$), the following non-linear form results

$$\left[\theta_1\right]_{T_T \to 0} = \frac{1}{\rho}\left(\frac{\sqrt{1 + \rho} - 1}{\sqrt{2} - 1}\right) \tag{37}$$

Curves for intermediate temperatures can be obtained from Eq. (35) using the experimental values of b_{std} from Fig. 6.

The data are compared to the predictions of the second order model on Fig. 13. None of the data show evidence of bowing away from the 45° line, even for target temperatures of 1700°K. Such bowing should have been

observed if the second order model described the dissociation process.

The first order model, on the other hand, predicts for all target temperatures

$$\theta_1 = 1/\rho \qquad (38)$$

This relation quite adequately represents the data on Fig. 13 .

Effect of Beam Composition

The variation of the mass two and mass four signals with target temperature were measured for a pure D_2 beam. The results were similar in all respects to those for pure H_2 beams shown on Figs. 4 and 5 .

Mixed H_2-D_2 beams were generated by adding a prepared 50-50 mixture to the source by the mechanical leak. Because of the square root of mass effect in channel effusion, the H_2:D_2 ratio in the mixed beam was $\sqrt{2}$:1 In one experiment with this beam, the mass two signal (which could represent H_2 or D) was monitored as the target temperature was increased. The resulting curve had a negative slope at low temperatures, passed through a minimum at T_T = 1600°K, and increased at higher temperatures until a plateau was reached. In effect, the curve was nothing more than a superposition of Fig. 4 for pure H_2 and the analog of Fig. 5 for deuterium. The minimum at 1600°K coincided with the onset to D_2 dissociation as observed in the experiment utilizing a pure D_2 beam. This behavior suggests that the two components of the mixed beam were interacting with the surface quite independently of one another.

To verify this idea, HD formed by the surface exchange reaction from a mixed beam was sought by monitoring the mass three signal as the target

temperature was increased from 300 to 2500°K. Bergsnov-Hanson and Pasternak[7] noted that traces of CO on the surface inhibited the exchange reaction, and that extensive temperature cycling of the filament was necessary before HD could be detected. A similar cleaning program was followed here, and included short term thermal cycling and long bake-outs of the target at 1800-2000°K. The target temperature was then reduced to the desired value and a measurement of the mass three signal immediately made. Separate tests indicated that the time required for CO monolayer coverage was much larger than the time required to make a measurement. In the middle of the HD search program, a fresh tantalum foil was inserted, but the results were unchanged.

In all of the mixed beam experiments, the mass three signal was two orders of magnitude less than the maximum mass one signal observed with the pure H_2 beams. The HD signal level was barely above the noise level of the detection system. We suspect that the mass three signals indicate a trace HD impurity in the premixed gas rather than the product of surface exchange between the H_2 and D_2 in the primary beam. Target temperatures in the range 300-800°K (measured by the resistance of the target foil) were of particular interest, since Bergsnov-Hanson and Pasternak found substantial exchange on molybdenum in this range. We found no modulated HD emitted from the tantalum target at any temperature. Although the target produced no HD, the ion pump very quickly produced substantial quantities for the background gas as soon as the mixed beam was turned on.

In order to determine whether a much higher pressure would produce HD by surface exchange on tantalum, the Knudsen cell source (which was also made of tantalum) was heated while a mixed beam was effusing through

the channels. The total pressure in the source was 3 torr, compared to 3×10^{-7} torr equivalent pressure of the beam at the target location. No HD was observed until the source has been heated to ~ 900°K, at which point HD reflected by the cold target was first observed. The mass three signal increased rapidly until 1400°K. At higher temperatures, the signal remained constant with further increase in source temperature. The strength of the HD signal at this plateau was comparable to the maximum mass one signal observed with pure H_2 beams on hot targets. This experiment suggests that above 1400°K an equilibrium mixture of H_2, HD, and D_2 was present in the Knudsen cell source, but that even with 3 torr total pressure, a tantalum surface needs to be heated to ~ 900°K before the exchange reaction commences at an appreciable rate. In view of these results it is not surprising that no HD was observed at 3×10^{-7} torr.

A Simple Model

Previous work on the interaction of hydrogen on metals has shown that the desorption of molecular hydrogen from the surface is second order in the surface concentration.[5,9,22] This is interpreted as indicative of the presence on the surface of highly mobile atoms which act as a two-dimensional gas. Sufficiently energetic collisions result in reconstitution of molecular species which then evaporate. Once an atom enters the mobile surface state, it retains no memory of its original partner, and can recombine with any other adsorbed atom. In particular, if the surface population is half H and half D, an adsorbed atom has an equal probability of colliding with either isotope. This results in evaporation of molecular species in equilibrium proportions, in which the H_2:HD:D_2 ratio is approximately 1:2:1.

On the other hand, if the mobility of the adsorbed atoms is low, the

desorbed molecular species arise primarily from recombination of adjacent adatoms which were the original partners in the chemisorbed molecule. Re-emission of molecular hydrogen by this process is first order in the adatom pair concentration, and in the case of mixtures of hydrogen and deuterium, surface exchange will not occur.

Both of these mechanisms of molecular reconstitution are combined in the following simple model of the surface process.

Adsorbed atoms are supplied by dissociative adsorption of impinging gas phase molecules

$$H_2(g) \longrightarrow (H---H) \tag{39}$$

where (H---H) represents two adatoms on adjacent lattice sites. The rate of this process is given by Eq. (7).

The species (H---H) can either recombine and evaporate as a molecule or jump apart and enter the surface diffusion process. The probability that the former occurs is denoted by ϵ, and results in first order molecular recombination

$$(H---H) \longrightarrow H_2(g) \tag{40}$$

Although this process involves prior dissociative adsorption of molecular hydrogen, it can be regarded as a completely efficient energy accommodation process. It differs from the purely elastic reflection of hydrogen from the surface, which does not involve bond rupture and is characterized by a temperature-independent sticking probability and very inefficient thermal accommodation. First order recombination, on the other hand, is strongly

temperature dependent. The rate at which this process occurs is

$$R_{21}^{E} = \eta_2 \epsilon I_T \qquad (41)$$

where R_{21}^{E} denotes the rate of evaporation of molecular hydrogen by a first order mechanism.

The fraction $1-\epsilon$ of the chemisorbed hydrogen which does not immediately re-evaporate as molecules enters the surface diffusion process

$$(H---H) \longrightarrow 2(H) \qquad (42)$$

where (H) represents an isolated atom on the surface. The rate of this step is $\eta_2(1-\epsilon)I_T$.

The migration of adatoms on the surface consists of jumps from one lattice site to another in a purely random manner. Upon each jump, there is a probability β that the atom will leave the surface and enter the gas phase before being secured onto another lattice site

$$(H) \longrightarrow H(g) \qquad (43)$$

If the jump frequency is denoted by ν, the probability of atom evaporation per second is $\beta\nu$, which is equal to the first order rate constant k_1^E. If there are n atoms/cm^2 in this process, the macroscopic rate of atom emission is given by Eq. (8).

If the migrating atom does not evaporate as an atom, it can be removed from the surface only by collision with another migrating adatom to form molecular hydrogen

$$(H) + (H)_f \longrightarrow H_2(g) \qquad (44)$$

where the subscript f denotes an adatom which originated from a different chemisorbed molecule from the atom with which it reacts. For low, uniform surface coverage, the probability that after a jump a wandering adatom finds itself adjacent to another adatom is n/n_s, where n is the surface concentration and n_s is the number of sites per cm^2. If two adatoms are adjacent to each other, the probability of combination is ϵ, just as in the recombination of original partner atoms. The combined probability that a migrating adatom will recombine and evaporate as molecular hydrogen per jump is $\left(n/n_s\right)\epsilon$. If there are n adatoms/cm^2 performing such random jumps, the macroscopic rate of second order molecular hydrogen emission is

$$R_{22}^E = \left(n/n_s\right)\epsilon\nu n = 4D_s\epsilon n^2 \qquad (45)$$

where the number of sites/cm^2 has been taken as the reciprocal of the square of the distance between sites, $1/d^2$, and the surface diffusion coefficient introduced

$$D_s = \tfrac{1}{4}\nu d^2 \qquad (46)$$

R_{22}^E is the rate of molecular hydrogen emission due to the second order process of Eq. (44). The total rate of molecular hydrogen emission, R_2^E, is the sum of R_{21}^E and R_{22}^E. The rates of dissociative adsorption, atom emission, and molecular evaporation are related by the material balance of Eq. (10). With this restriction, the rate of molecular evaporation becomes

$$R_2^E = R_{21}^E + R_{22}^E = \tfrac{1}{2}\left(\frac{\epsilon}{1-\epsilon}\right)k_1^E n + 4D_s\left(\frac{\epsilon}{1-\epsilon}\right)n^2 \qquad (47)$$

The first term on the right of Eq. (47) is the contribution of first order hydrogen formed by recombination of the original chemisorbed partners, while the last term represents the rate of molecular hydrogen formation by second order recombination of surface atoms randomly chosen from the surface population. Using Eqs. (7), (8), and (47) in Eq. (10) yields

$$R_1^E = \tfrac{1}{4}\left[\frac{\left(k_1^E\right)^2}{4D_s\epsilon}\right]\left\{\sqrt{1 + 16\eta_2 I_T(1-\epsilon)\left[\frac{4D_s\epsilon}{\left(k_1^E\right)^2}\right]} - 1\right\} \qquad (48)$$

If the term $4D_s\epsilon/\left(k_1^E\right)^2$ is small because of low atom mobility or if ϵ is close to unity because the probability of localized recombination is large, Eq. (48) reduces to Eq. (11) in which k_2^E is given by the coefficient of n in Eq. (47). This is the pure first order limit.

If the probability of recombination of adjacent atoms is low ($\epsilon \ll 1$), Eq. (48) reduces to the pure second order model given by Eq. (12) in which k_2^E is identified with $4D_s\epsilon$.

The model embodied in Eq. (48) is neither pure first or second order, but contains these two cases as limits when the parameters of the surface interaction assume certain values. The data obtained in the present study indicate that the hydrogen-tantalum system follows the first order model at all temperatures and pressures studied. One reason for this behavior may be the presence of heterogeneities or patches on the surface.[6] A chemisorbed molecule may be trapped in a patch on the surface which restricts the migration of the adatoms and prevents rapid mixing on the surface. If

an impinging gas phase molecule chemisorbs on a vacant patch (which is likely at the very low coverages characteristic of high surface temperatures), and the mean time for the escape of an adatom from the patch is large, the adatoms will either evaporate as atoms or recombine with each other.

The apparent first order behavior may also be due to bulk solution of the adatoms. The hydrogen pressure (or impingement rate) is greater on the front face of the target than on the back face, due to the presence of the molecular beam. For the standard beam, the total pressure on the front face is $\sim 6\times10^{-7}$ torr (beam plus background) while on the back face, the pressure is 3×10^{-7} torr (background only). The adatom concentration on the front face should be approximately twice that on the back face. Assuming a Henry's law constant relating the concentrations of adatoms and dissolved atoms just beneath the surface, a driving force for bulk diffusion of hydrogen through the foil exists. The disappearance of H atoms from the surface by bulk dissolution and diffusion constitutes a sink for the surface population and reduces the surface concentration below the value which would exist if the body of the tantalum were impervious to hydrogen.

The final result of including this additional mode of hydrogen removal from the surface in the preceding analysis is to replace k_1^E in Eqs. (47) and (48) by $k_1^E + D_V H/2\ell$, where H is the Henry's law constant (which, when combined with the adsorption isotherm gives the bulk solubility as a function of pressure), D_V is the bulk diffusion coefficient, and ℓ is the thickness of the foil (0.001 in). If the term $D_V H/2\ell$ is comparable in magnitude to k_1^E, Eq. (48) can more readily be approximated by its first order limit. Langmuir[2] has proposed the existence of a dissolved gas phase in metals at elevated temperatures, and Moore and Unterwald[8,9] have demonstrated appreciable

high temperature solution of hydrogen in tungsten and molybdenum. Since tantalum has a larger capacity for hydrogen than tungsten or molybdenum (at low temperatures), bulk dissolution may have a crucial effect on the surface processes.

Even if removal of surface hydrogen by diffusion through the foil is not significant, the high solubility of hydrogen in tantalum could be responsible for the inability to detect HD in the mixed beam experiments. Upon dissociative adsorption, an appreciable fraction of the adatoms may be submerged in the bulk metal for a significant period of time before reappearing at the surface and recombining to form a molecular species. If the average time spent in the bulk is large compared to the 20 msec modulation time of the primary molecular beam, the resulting molecular species will be completely demodulated and appear as an undetectable dc signal in the phase sensitive detector.

SUMMARY

The dissociation of hydrogen on tantalum has been investigated by modulated molecular beam-mass spectrometric techniques and the results compared to first and second order models. Because of the phase sensitive detection method employed, the effect of the unmodulated hydrogen background in the vacuum system had to be taken into account in interpreting the data by the second order model. The discussion emphasized the atom emission rates, since these are not influenced by the unknown thermal accommodation and specular reflection effects which complicated the analysis of the reflected molecular hydrogen signals.

Based upon variation of the target temperature, beam temperature, beam intensity, and beam composition, the first order model was found to most adequately fit the data. The absence of HD in the mixed beam experiments in particular indicated that surface exchange was not significant at the temperatures and pressures investigated.

The first order kinetic analysis of the data yielded a 65 kcal/mole binding energy of atomic hydrogen on tantalum. The maximum sticking probability of molecular hydrogen on fresh polycrystalline tantalum was found to be 0.49, but this figure does not account for thermal accommodation or specular reflection. The apparent sticking probability increased for targets which had been subject to grain growth and exposed to carbon-bearing impurities. The sticking probability increased slightly with beam temperature in a manner characterized by an activation energy of 1.4 kcal/mole.

A simple model of the surface process which contained both pure first and second order behavior as limiting cases was proposed. According to this model, non-equilibrium first order kinetics is due either to low atom

mobility or a high probability of localized recombination. This may have been the result of patchy surfaces which created barriers to surface migration or of bulk solution of surface adatoms in the metal. The latter phenomenon may be the source of the unique behavior of tantalum among the metals for which interaction with hydrogen has been investigated.

ACKNOWLEDGMENTS

This work was supported by the United States Atomic Energy Commission.

REFERENCES

1. I. Langmuir, J. Am. Chem. Soc. 34, 1310 (1912).
2. I. Langmuir, J. Am. Chem. Soc. 37, 417 (1915).
3. I. Langmuir, Gen. Elec. Rev. 29, 153 (1926).
4. W. F. Giaugue, J. Am. Chem. Soc. 52, 4816 (1930).
5. D. Brennan and P. C. Fletcher, Proc. Roy. Soc. A250, 389 (1959).
6. T. W. Hickmott and G. Ehrlich, J. Phys. Chem. Solids 5, 47 (1958).
7. B. Bergsnov-Hansen and R. A. Pasternak, J. Chem. Phys. 45, 1199 (1966).
8. G. E. Moore and F. C. Unterwald, J. Chem. Phys. 40, 2626 (1964).
9. G. E. Moore and F. C. Unterwald, J. Chem. Phys. 40, 2639 (1964).
10. J. N. Smith and W. L. Fite, J. Chem. Phys. 37, 898 (1962).
11. J. N. Smith and W. L. Fite, Advances in Rarified Gas Dynamics (Academic Press, New York, 1963) Supplement 2, Vol. 1, p. 430.
12. G.S. Holister, R.T. Brackmann and W.L. Fite, J. Chem. Phys. 34, 1572 (1961).
13. S. Datz, G. E. Moore and E. H. Taylor, Advances in Rarified Gas Dynamics (Academic Press, New York, 1963), Supplement 2, Vol. 1, p. 347.
14. J. Perel, R. H. Vernon and H. L. Daley, J. Appl. Phys. 36, 2157 (1965).
15. M. Kaminsky, Adv. Energy Conversion 3, 255 (1963).
16. J. D. McKinley, J. Chem. Phys. 40, 120 (1964).
17. R. A. Krakowski (Ph. D. Thesis), University of California, Berkeley, UCRL-17336, 1967.
18. J. G. King and J. R. Zacharias, Adv. in Electronics and Electron Phys. 6, 1 (1956).
19. J. A. Giordmane and T. C. Wang, J. Appl. Phys. 3, 463 (1960).
20. G. R. Hanes, J. Appl. Phys. 3, 2171 (1960).

21. G. Ehrlich, J. Chem. Phys. 31, 1111 (1959).

22. T. W. Hickmott, J. Chem. Phys. 32, 810 (1960).

23. D. R. Stull and G. C. Sinke, Thermodymanic Properties of the Elements (American Chemical Soc., Washington, D.C., 1959). These values are the square root of those required here.

24. N. Eisenstadt and S. A. Hoenig, J. Chem. Phys. 45, 127 (1965).

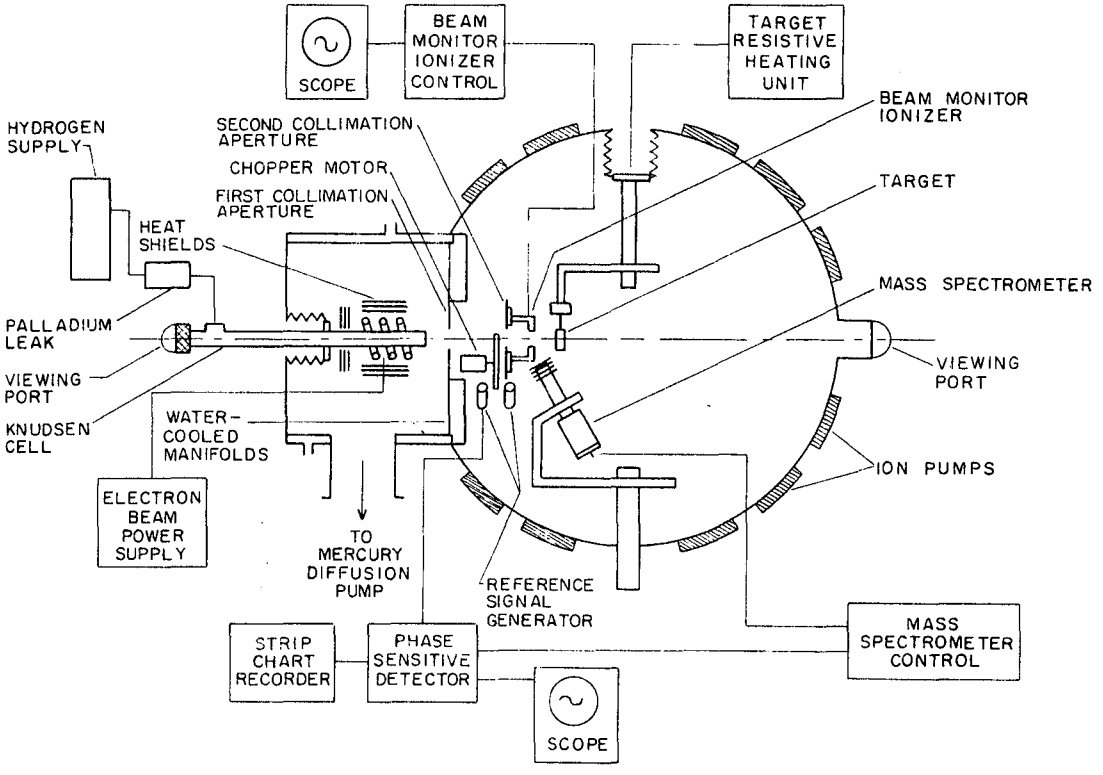

XBL 672-551

Fig. 1 Molecular beam-mass spectrometric apparatus

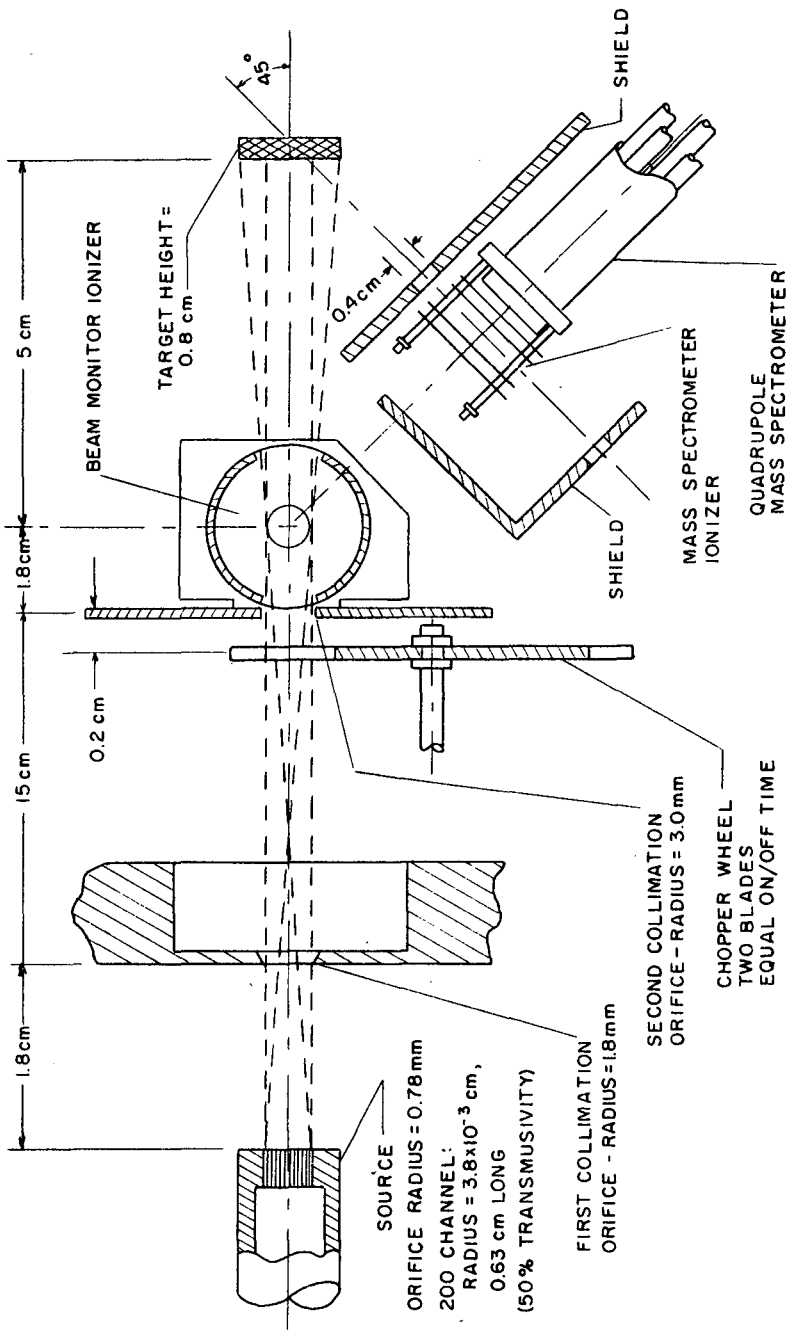

XBL 672-1167

Fig. 2 Schematic of beam geometry

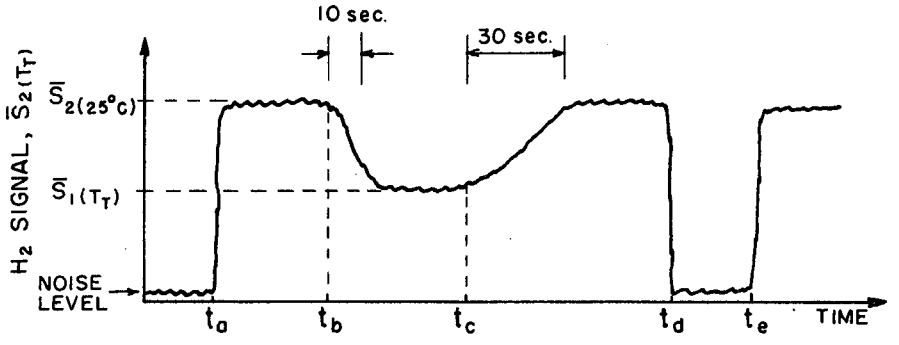

t_a BEAM ON; TARGET AT ROOM TEMPERATURE

t_b TARGET HEATED TO T_T

t_c TARGET COOLED; NOTE LONGER TIME NEEDED TO RECOVER ROOM TEMPERATURE LEVEL

t_d TARGET REMOVED

t_e TARGET REPLACED

A. MASS TWO SIGNAL TRACE.

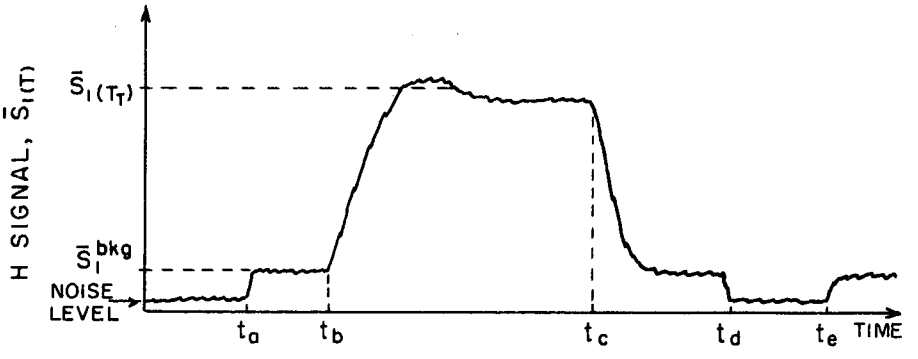

t_a BEAM ON; TARGET AT ROOM TEMPERATURE

t_b TARGET HEATED

t_c TARGET COOLED

t_d TARGET REMOVED

t_e TARGET REPLACED

B. MASS ONE SIGNAL TRACE.

XBL 672-587

Fig. 3 Typical signal traces during target temperature variation

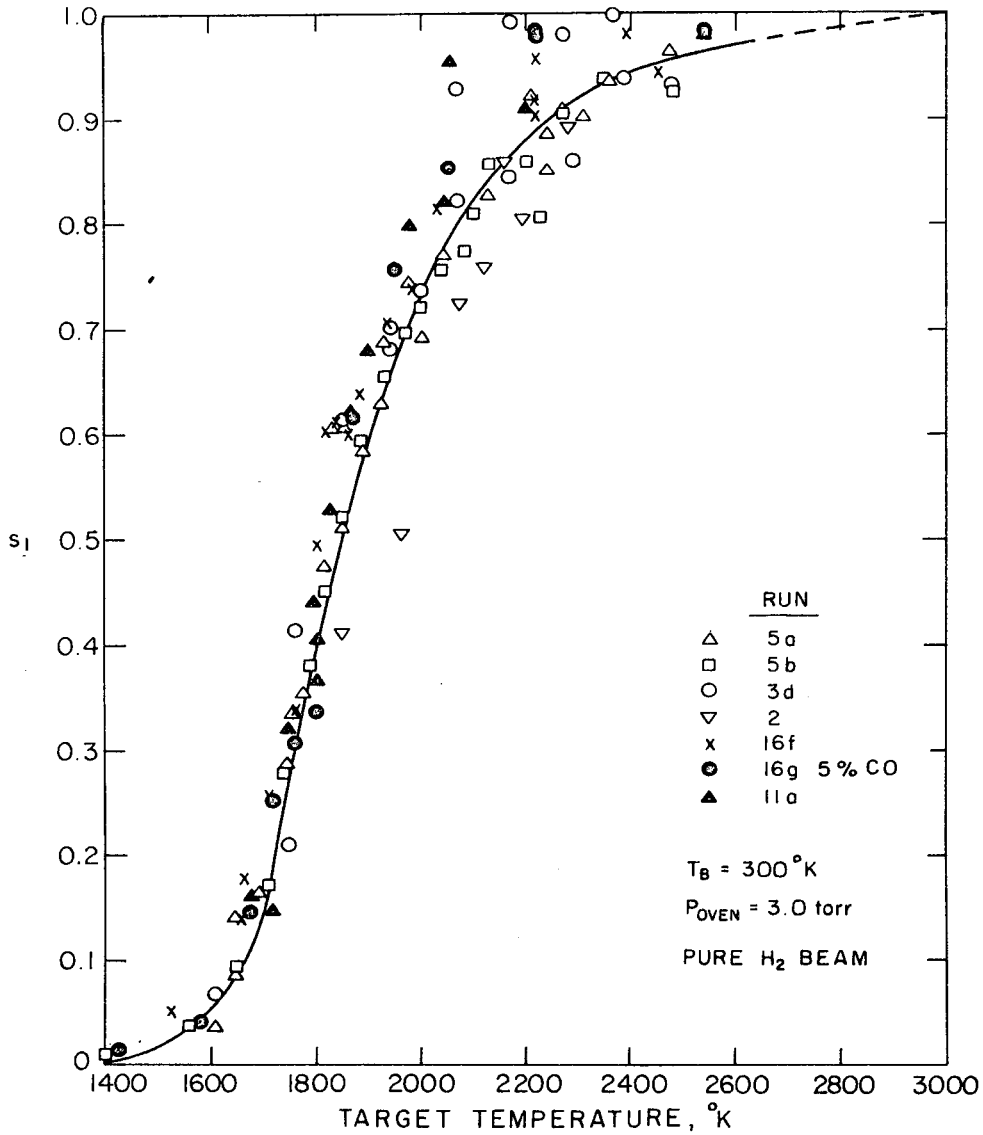

XBL 672-595

Fig. 4 Normalized atomic hydrogen emission as a function of target temperature

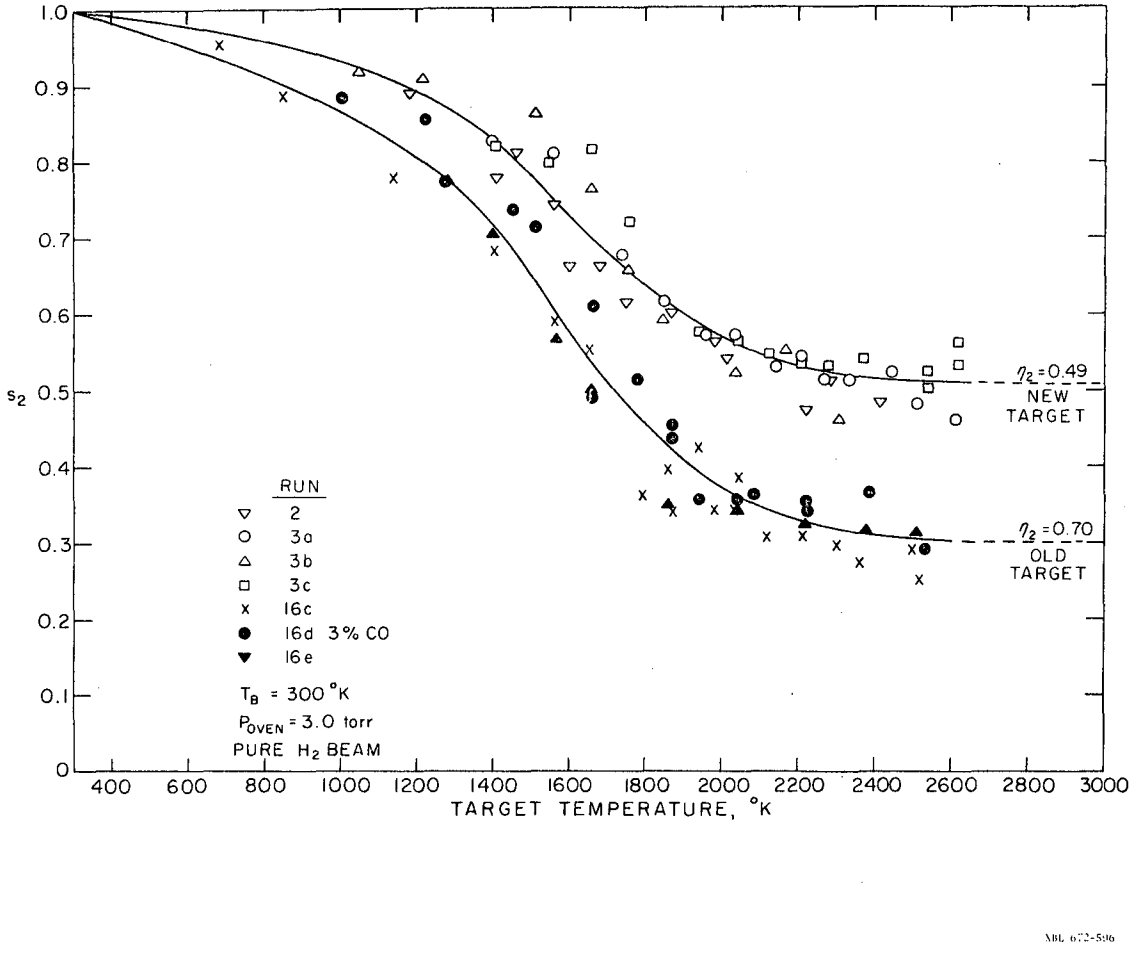

MBL 672-536

Fig. 5 Normalized molecular hydrogen signal as a function of target temperature

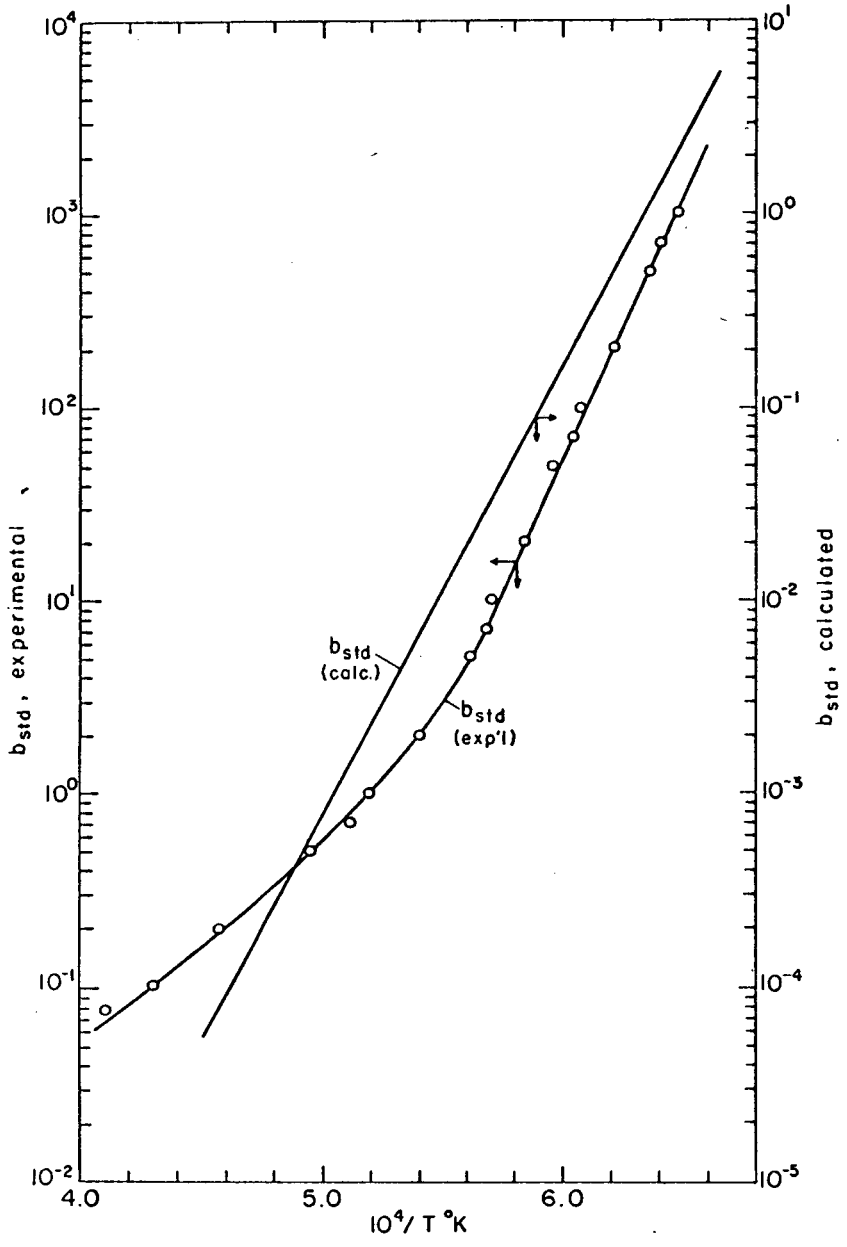

Fig. 6 Comparison of experimental values of the parameter b with the predicted values from equilibrium second order theory for the standard beam.

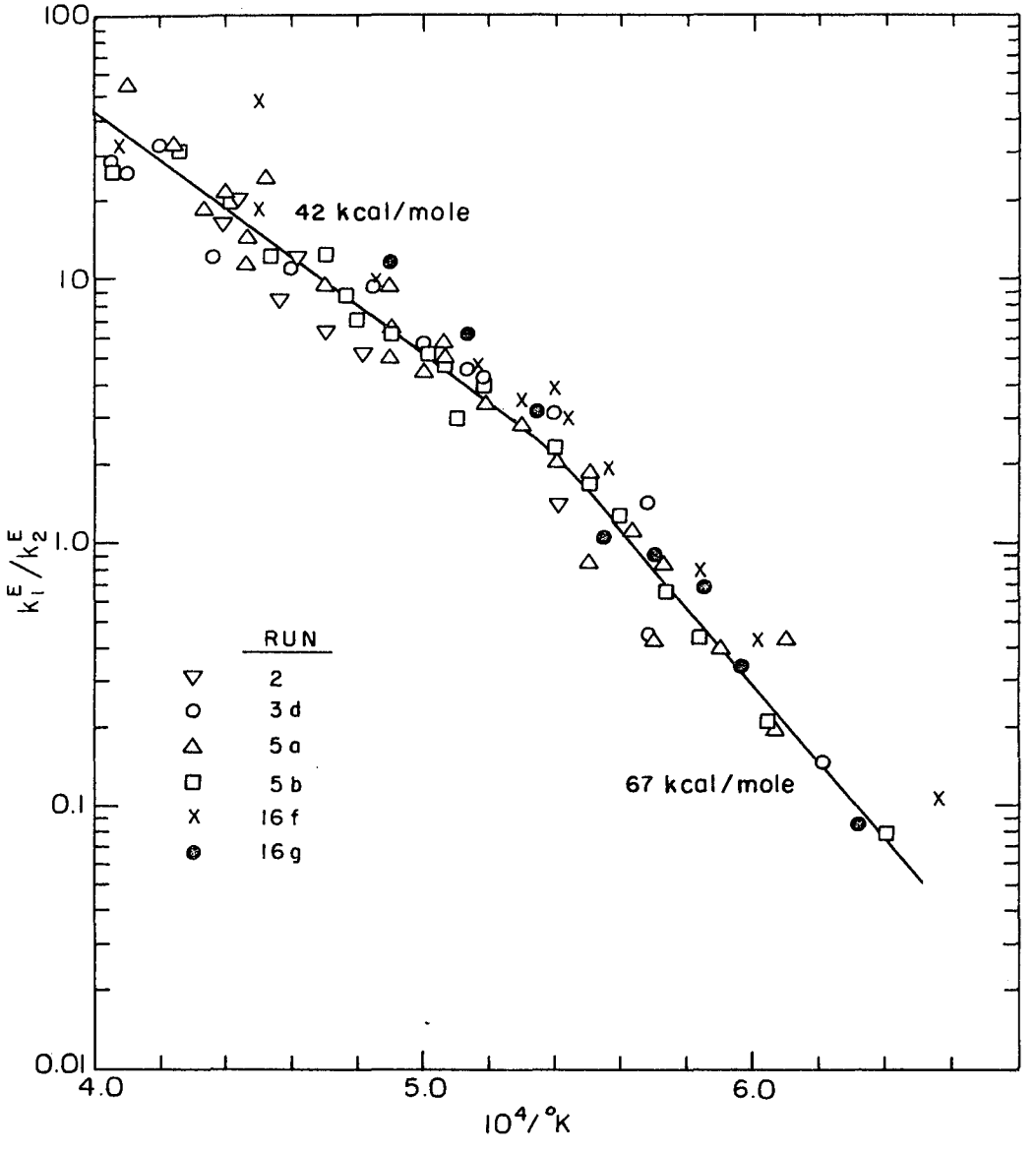

XBL 672-1169

Fig. 7 Analysis of atomic hydrogen data by the first order model.

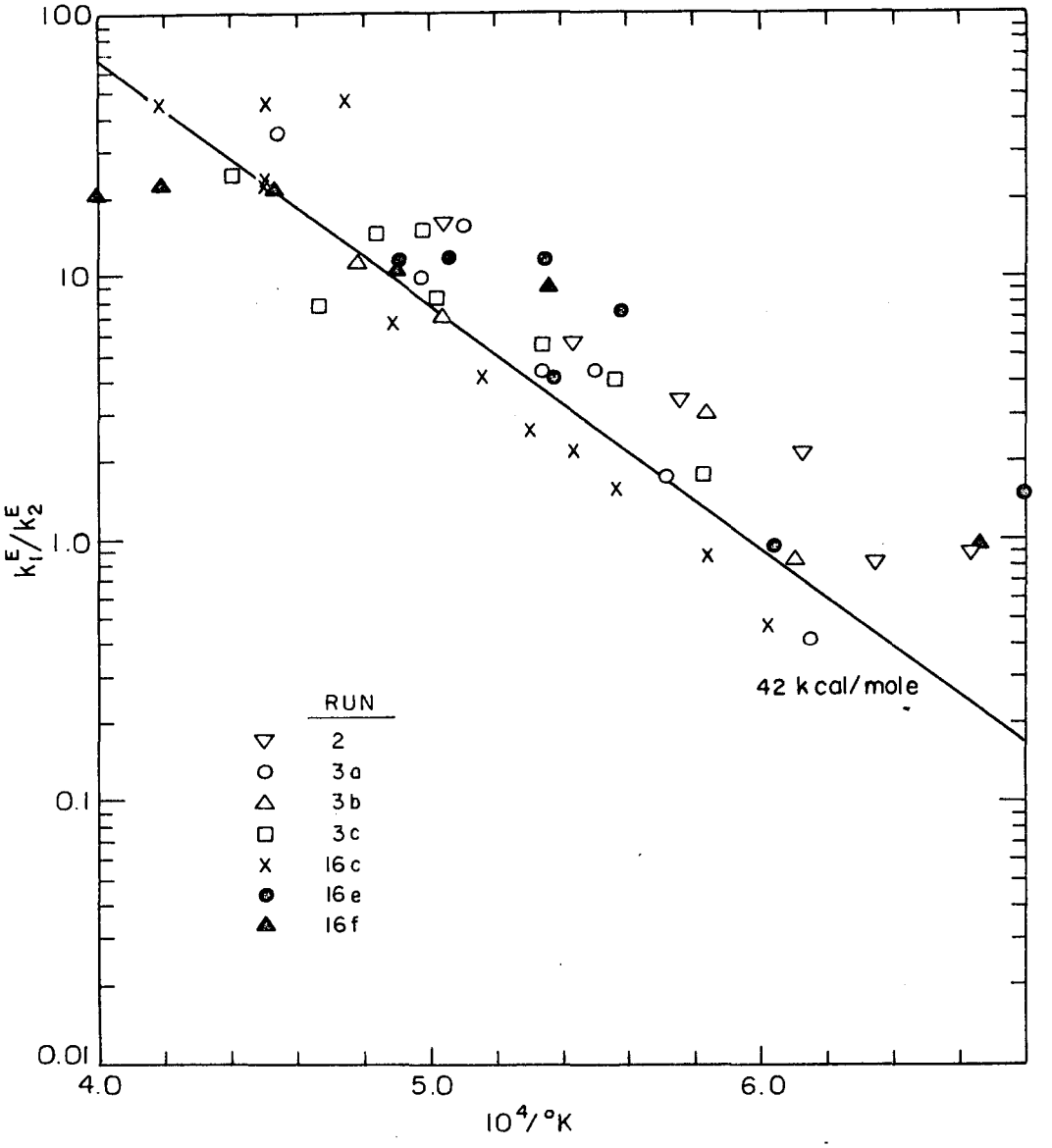

XBL 672-1168

Fig. 8 Analysis of the molecular hydrogen data by the first order model

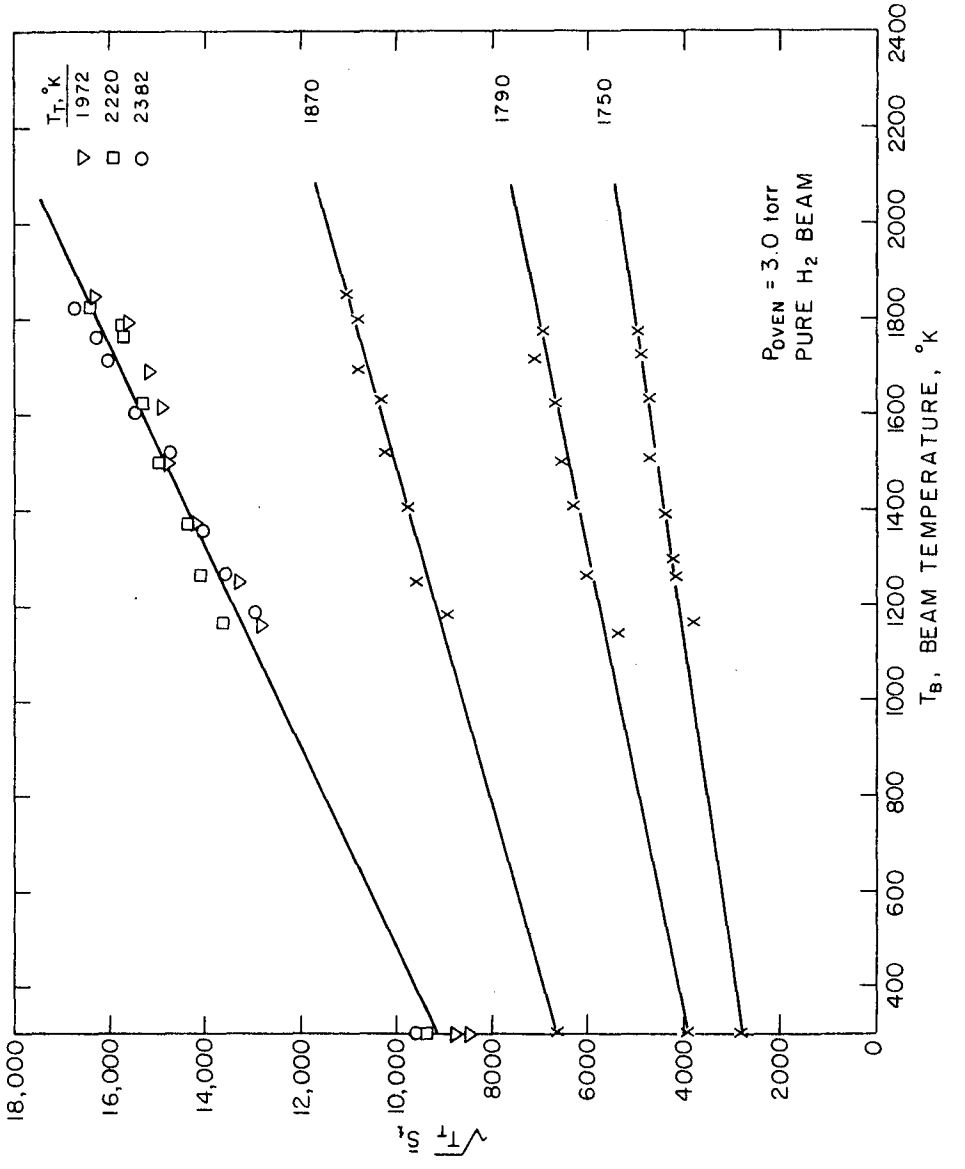

Fig. 9 Effect of beam temperature on the atomic hydrogen signal

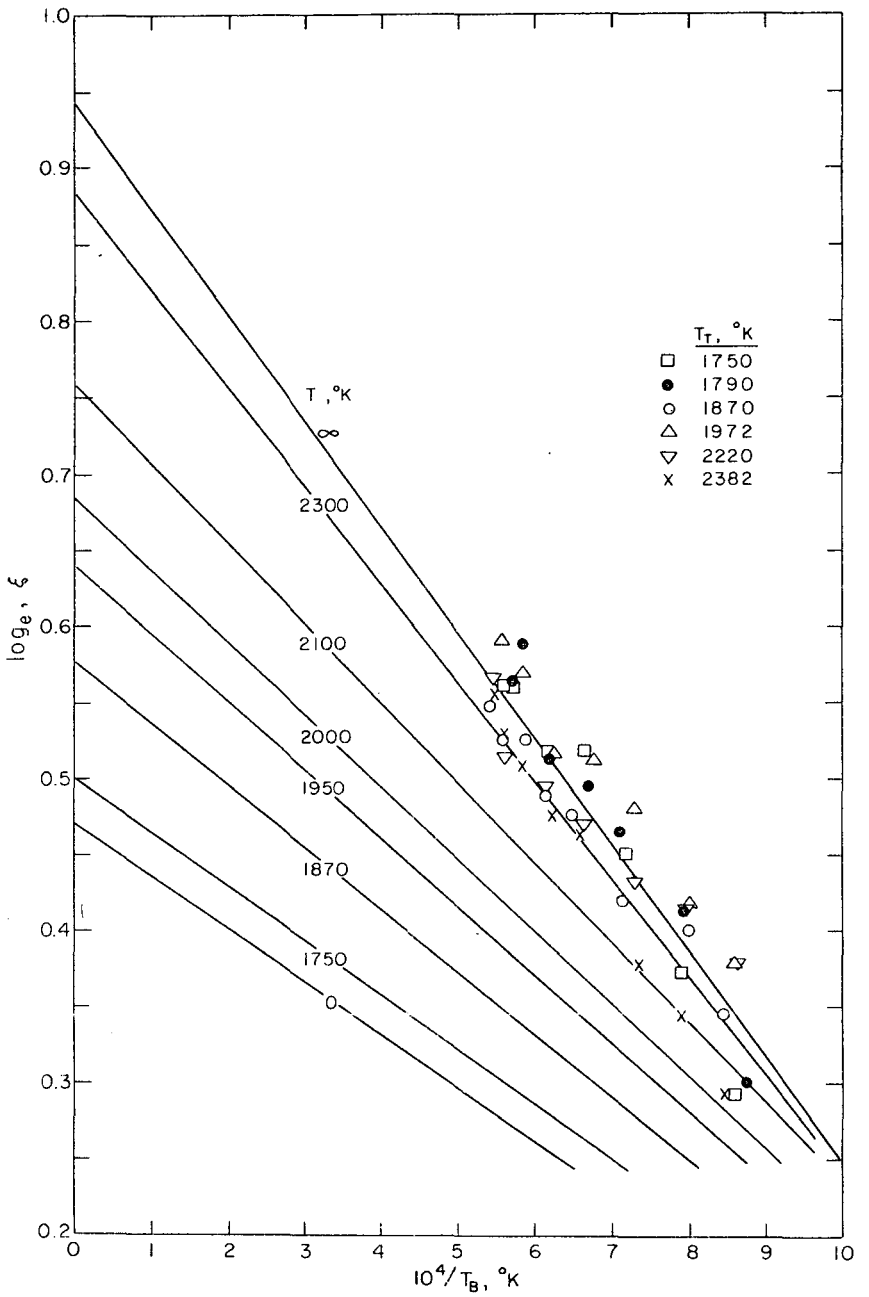

XBL 672-1171

Fig. 10 Comparison of theoretical and experimental effects of beam temperature on the atomic hydrogen emission rate

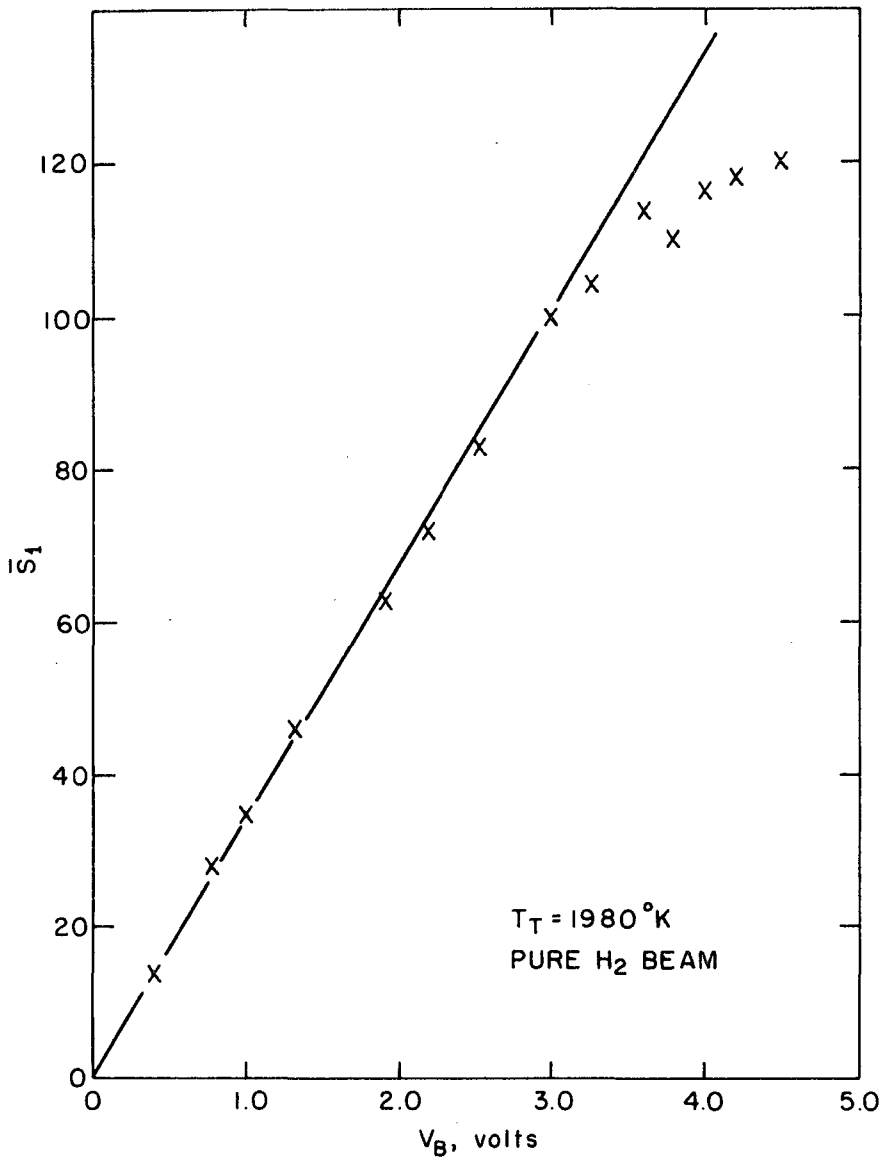

XBL 672-1184

Fig. 11 Variation of the rate of atomic hydrogen emission with beam intensity at a fixed target temperature

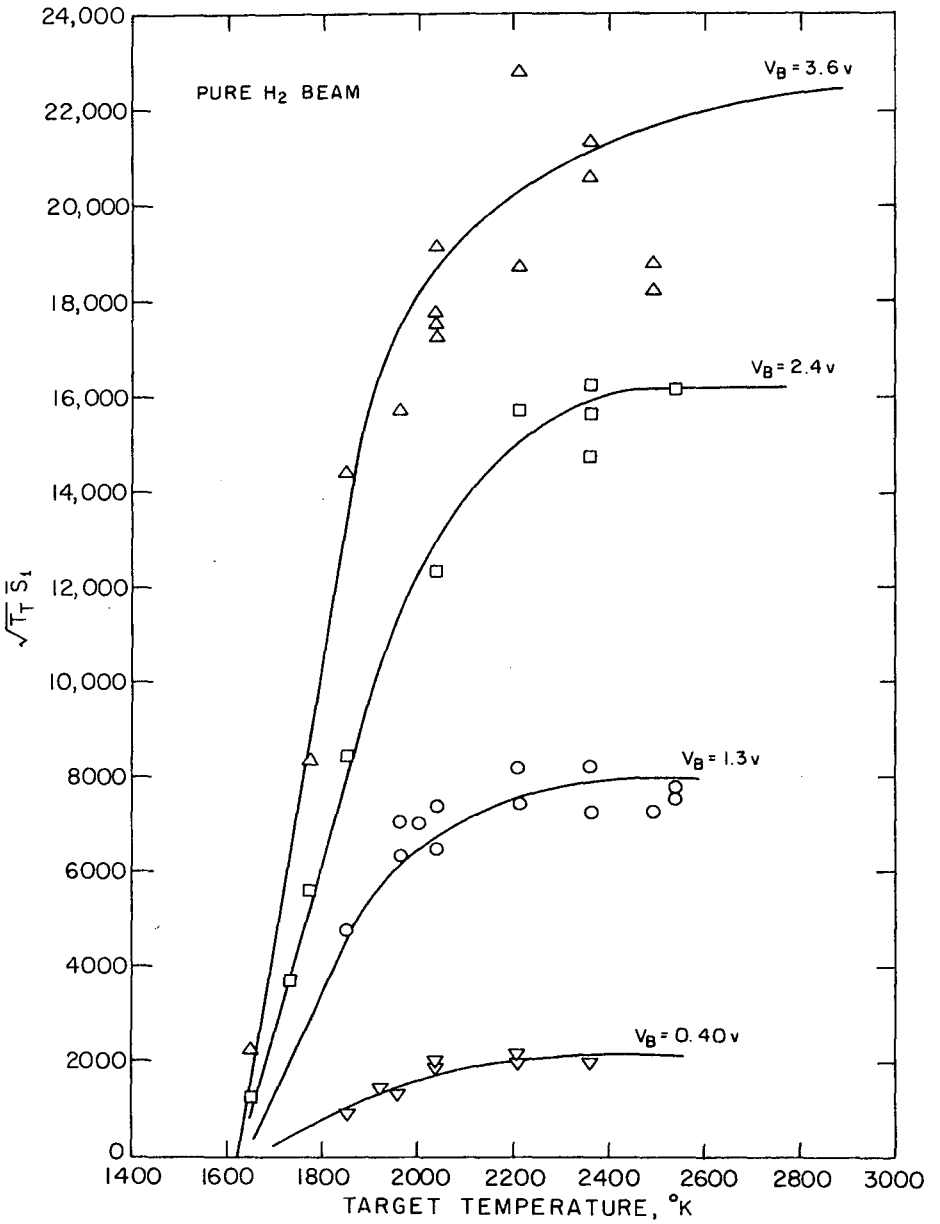

XBL 672-1166

Fig. 12 Variation of the rate of atomic hydrogen emission with target temperature for four beam intensities

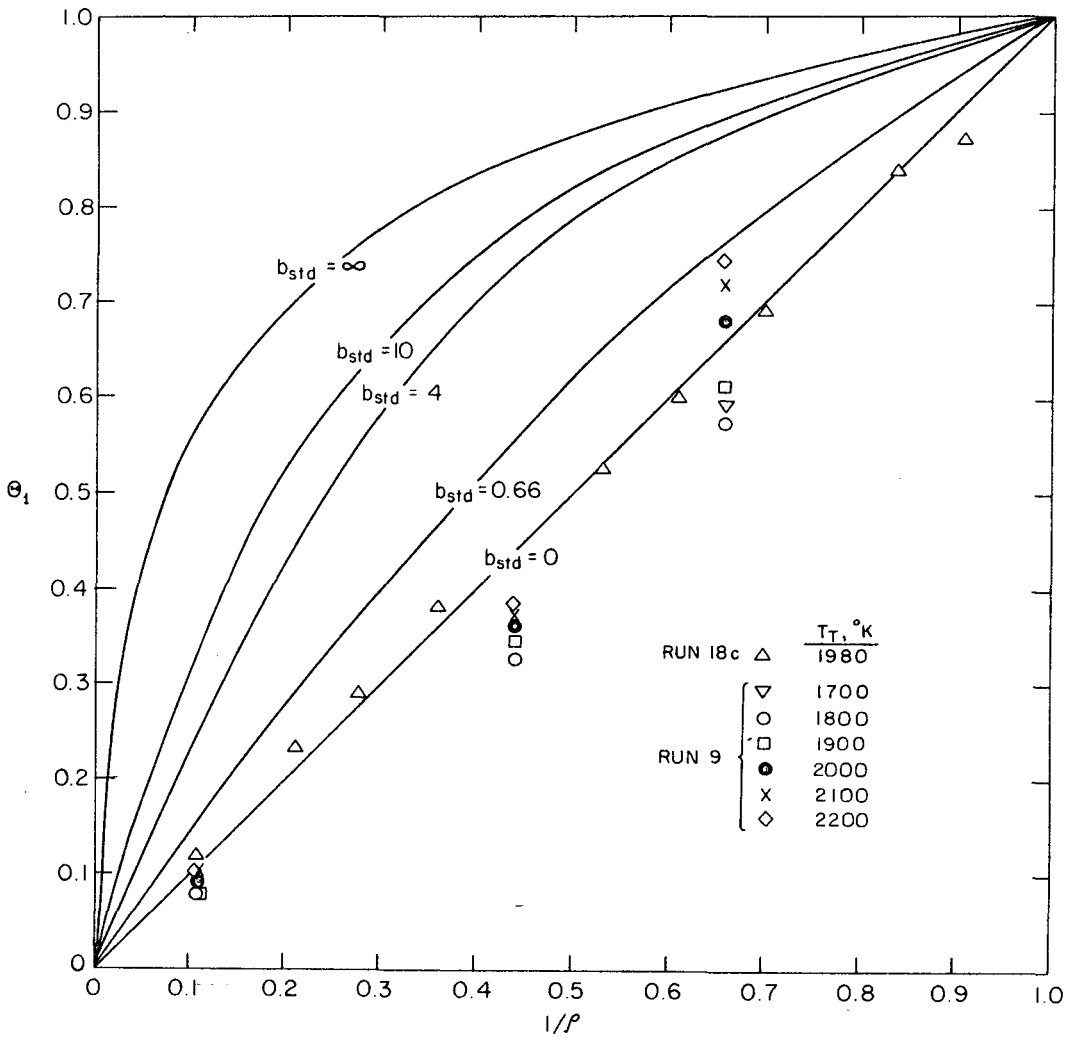

XBL 673-1222

Fig. 13 Normalized atomic hydrogen emission rate as a function of beam intensity relative to the standard beam.